ADVANCED FUNCTIONAL MATERIALS
www.afm-journal.de



# Channeled β-TCP Scaffolds Promoted Vascularization and Bone Augmentation in Mandible of Beagle Dogs

*Tao Yu, Qing Liu, Ting Jiang,* Xuesong Wang, Yunzhi Yang, and Yunqing Kang**

**A major hindrance to successful alveolar bone augmentation and ridge preservation using synthetic scaffolds is insufficient vascularization in the implanted bone grafts. The slow ingrowth of host vasculature from the bone bed of alveolar bone to the top of the implanted bone grafts leads to limited bone formation in the upper layers of the implanted grafts, which hinders the subsequent implantation of titanium dental implants. In this study, macroporous beta-tricalcium phosphate (β-TCP) scaffolds with multiple vertical hollow channels are fabricated that play a similar role as blood vessels for nutrient diffusion and cell migration. The results show that the hollow channels accelerate the degradation rate of the β-TCP scaffolds and the in vitro release of a bone forming peptide-1, which significantly promote proliferation and osteogenesis of human bone mesenchymal stem cells on the channeled scaffolds, compared to nonchanneled scaffolds in vitro. More volume of newly formed bone tissues with more blood vessels are augmented in the channeled scaffolds when implanted in mandibular bone defects of beagle dogs. Channeled scaffolds significantly promote new bone formation and augment the height of the mandible. These findings indicate channeled scaffolds facilitate vascularization and bone formation and have great potential for vascularized bone augmentation.**

## 1. Introduction

After tooth extraction, inevitable and irreversible alveolar ridge resorption and alveolar bone loss horizontally and vertically are frequently observed phenomena,[1,2] which may either impair the final esthetic outcomes or fail to provide sufficient bone volume support for future screw dental implants placement.[3] To prevent ridge resorption and postextraction alveolar bone loss, immediate or early implant placement procedures have become a key component and standard-of-care treatment following tooth removal in clinical dentistry.[4]

Several clinical techniques and many biomaterials have been introduced in an effort to preserve alveolar ridge and promote bone augmentation for following dental implants.[5–7] In these strategies, autologous bone grafts or allografts are extensively used for bone grafting of the socket in dentistry. However, limited supply, donor site morbidity, prolonged recovery, and complicated surgical procedures hamper their applications in immediate or early implant placement of a socket after tooth extraction.[8–10] A synthetic bone substitute Bio-Oss collagen has been extensively used for horizontal bone augmentation. However, clinical results indicated that its ability for vertical bone augmentation was insufficient, and that dental implants placed in bone augmented with Bio-Oss showed an increased failure rate and a prolonged healing time due to insufficient bone volume.[11] Although other synthetic biomaterials options as alternative solutions have been extensively studied to treat a variety of bone defects in the past decades,[12–14] none of the bone grafting options currently available to preserve alveolar ridge and bone augmentation have an ideal outcome.[15,16]

Dr. T. Yu, Dr. Q. Liu, Prof. T. Jiang
Department of Prosthodontics
School and Hospital of Stomatology
Peking University
22# Zhong Guan Cun South Street, Beijing 100081, China
E-mail: ting-139@139.com
Dr. T. Yu
First Clinical Division
School and Hospital of Stomatology
Peking University
37# Xishiku Street, Beijing 100034, China
Dr. T. Yu, Dr. Q. Liu, Prof. T. Jiang
National Engineering Laboratory for Digital and Material Technology of Stomatology
Beijing Key Laboratory of Digital Stomatology
22# Zhong Guan Cun South Street, Beijing 100081, China
X. Wang
Department of Ocean and Mechanical Engineering
Florida Atlantic University
Boca Raton, FL 33431, USA
Prof. Y. Yang
Department of Orthopaedic Surgery
Department of Materials Science and Engineering
Department of Bioengineering
Stanford University
Stanford, CA 94305, USA
Prof. Y. Kang
Department of Ocean and Mechanical Engineering
Department of Biomedical Science
Florida Atlantic University
Boca Raton, FL 33431, USA
E-mail: kangy@fau.edu

DOI: 10.1002/adfm.201602631

In our published studies,[17] we used our template-casting method to create a porous beta-tricalcium phosphate porous scaffold ($\beta$-TCP). We implanted porous $\beta$-TCP scaffolds and autologous bone grafts into the mandible sites of rabbits. Results indicated that significant new bone formed in the scaffolds. Interestingly, we found that autografts showed a significant resorption after three months, while the porous $\beta$-TCP scaffolds kept the height, which strongly supported our hypothesis that porous scaffolds can augment the height of defective alveolar bone.[17] However, we also found that the bone density and bone volume percentage of newly formed bone in the implanted scaffolds was lower in the area away from the bone bed than that in the area near the bone bed in the mandible. This hinders the successful placement of following screw dental titanium implants. The main obstacle is that insufficient vascularization in the implanted grafts results in low bone volume formation.[18–22]

Studies have shown that although interconnected pores are essential and also required to facilitate nutrient diffusion and cell migration, pores alone cannot provide enough space and open/wide road and are insufficient for the vertical in-growth of host vasculature and nutrient diffusion.[23,24] As the maximum distance between the capillaries is around 200 μm,[25] oxygen and nutrients cannot be sufficiently supplied to thick constructs through only pores, which leads to necrosis and tissue death in the center of the implanted grafts.[26–28] Studies have shown that macrochannels effectively improved the nutrition diffusion and blood flow to the central zone of porous silk scaffolds, which significantly promoted formation of blood vessels compared with nonchanneled silk scaffolds.[29,30] Based on the reported results, it is plausible to conceive that an array of channels in a porous scaffold could robustly facilitate nutrient transportation and sufficient vascularization.

Besides the reported role of a channel structure in promoting vascularization, many studies have shown that angiogenic growth factors (vascular endothelial growth factor (VEGF), fibroblast growth factor (FGF), platelete-derived growth factor (PDGF), etc.) play a key role in inducing neovascularization during the process of new bone formation. Recently, studies have shown that a peptide sequence, named bone forming peptide-1 (BFP-1) derived from an immature region of bone morphogenetic protein-7, not only enhanced bone regeneration by up-regulating the expression of alkaline phosphatase (ALP), CD44, osteocalcin, and Runx2 in mouse bone marrow stromal cells, but also increased VEGF receptor expression in endothelial cells.[31,32]

Therefore, in this study, we added BFP-1 into hollow-channeled porous $\beta$-TCP scaffolds for alveolar bone regeneration. We hypothesized that the addition of BFP-1 into hollow channeled $\beta$-TCP scaffolds can synergistically and robustly induce vertical ingrowth of blood vessels and promote osteogenesis of deployed $\beta$-TCP scaffolds. We used our developed template-casting method to make hollow-channeled porous $\beta$-TCP scaffolds and loaded BFP-1 onto the channeled $\beta$-TCP scaffolds.[33,34] We investigated the effect on proliferation and osteogenesis of human bone marrow derived mesenchymal stem cells in vitro, and implanted scaffolds into mandibular bone defects of beagle dogs to explore bone augmentation and vascular growth in vivo.

## 2. Results and Discussion

### 2.1. Morphologies and Degradation Rate of the Scaffolds with and without Channels

In this study, two types of porous $\beta$-TCP scaffolds were used. One type of scaffold has five hollow channels and the other does not. The digital pictures and a scanning electronic microscopy image show that the scaffolds have interconnected pores (**Figure 1**a–c). According to our previous reports, the pore size is around 350–500 μm, and the porosity is around 80%.[35] The pore size, porosity, interconnectivity, and other morphologic characters of scaffolds play an important role in engineered bone regeneration. High porosity and large pore size may improve nutrient diffusion and increase cell viability in scaffolds. Channels in the scaffolds could further significantly promote nutrients transportation. Bai et al. developed a modified freeze-casting technique to prepare gradient channel structures within hydroxyapatite ceramic scaffolds. They found that such a scaffold with gradient channel from 4.54 to 11.8 μm has a very unique capillary behavior that promoted the self-seeding of cells.[36] Radisic et al. fabricated a kind of scaffold with parallel channels 370 μm in diameter and 410 μm in interval distance, which increased the cell viability and promoted the differentiation of stem cells in the scaffolds.[37,38] The study of Rose et al. on a series of hydroxyapatite scaffolds with one single channel in four different diameters (421, 314, 198, 170 μm) suggested more cell penetrated in the scaffolds in larger diameter channels.[39] Sharaf et al. found that scaffolds with channels of 1 mm diameter could promote cell proliferation and function comparing to scaffolds with 2 mm diameter channels.[40] In the mandible, dental arteries and branches of inferior alveolar artery are nearly parallel to each other, and they are vertical to the alveolar process.[41] Considering the above points, we fabricated scaffolds with parallel vertical channels with 1 mm diameter (Figure 1a). The degradation rate result shows that channeled scaffolds had a significantly higher degradation rate in terms of the concentration of phosphate acid ions, compared to the porous scaffolds without channels (Figure 1d). This result implied that channels promoted the transportation of liquid so that the degradation happened faster.

### 2.2. In Vitro Release Profile of BFP-1

From the results of the study, channeled scaffolds degraded faster than nonchanneled ones. It indicated that the channels promoted the diffusion of phosphate, the byproduct of $\beta$-TCP degradation, and promoted the diffusion of nutrient. We measured the in vitro release of BFP-1 from the scaffolds after the BFP-1 was absorbed onto the scaffolds. Results indicate that the release of BFP-1 from channeled scaffolds was remarkably higher for 3 d than that from nonchanneled scaffolds. After 3 d, there is no significant difference between the two groups (Figure 1e). This result implies that channels in the scaffolds promoted the diffusion of fluids, which is beneficial to rapid blood supply once the scaffolds are implanted in vivo.



*Adv. Funct. Mater.* **2016**,
DOI: 10.1002/adfm.201602631

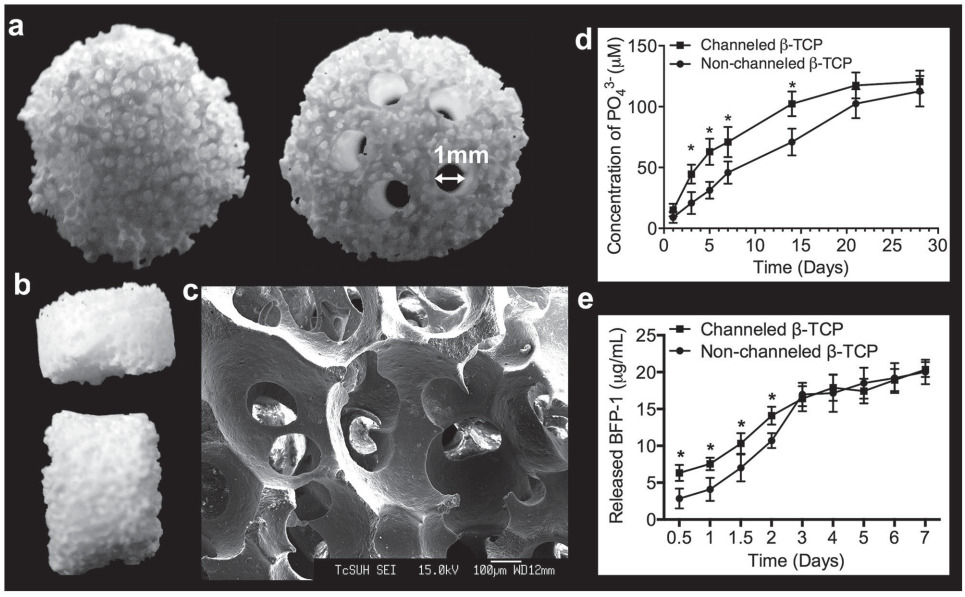


**Figure 1.** Digital pictures show two types of macroporous scaffolds, without hollow channels and with hollow channels (a: top view, and b: side view). Each channel has 1 mm diameter. c) A scanning electron microscopy (SEM) image shows the morphologies of interconnected pores. d) In vitro degradation measurement of phosphate ions ($PO_4^{3-}$) shows that channeled scaffolds degraded faster than nonchanneled scaffolds. e) In vitro release profile of BFP-1 also shows that channeled scaffolds promoted the release of BFP-1 during the first three days, in contrast with the nonchanneled scaffolds.

### 2.3. Proliferation and Differentiation of hBMSCs on Scaffolds

Human bone mesenchymal stem cells (hBMSCs) from the redundant cancellous bone amputated during orthognathic surgery were cultured on tissue culture plates, and showed spindle morphology after days. ALP staining indicated that a large number of cells presented a grey-black positive expression (**Figure 2**a). Alizarin red S staining showed that hBMSCs formed red calcium nodules (Figure 2b). Oil Red O staining further demonstrated that hBMSCs can differentiate into adipose cell type (Figure 2c). These results confirmed the multipotent differentiation abilities of hBMSCs. Afterwards, we loaded 100 μL cell suspension onto the porous scaffold. The cell suspension can penetrate into the pores of the scaffold. As the surface of the ceramic scaffold can absorb liquid so that all the cells in the cell suspension can attach on the surface of inner pores of the scaffold. Once the cells attached after about 1 h, we added enough culture medium to continue to culture cells.[34] Cell proliferation assay showed that channeled $\beta$-TCP scaffolds significantly promoted cell proliferation at day 3 and 5, regardless of the addition of BFP-1. However, there was no significant difference in cell proliferation of hBMSCs between BFP-1 groups and non-BFP-1 groups involved in channeled or nonchanneled scaffolds after 1, 3, 5, and 7 d of culture (Figure 2d).

The assay results of early osteogenic differentiation (ALP activity) showed that ALP activity at day 14 was significantly enhanced in scaffolds with BFP-1, compared to the same type

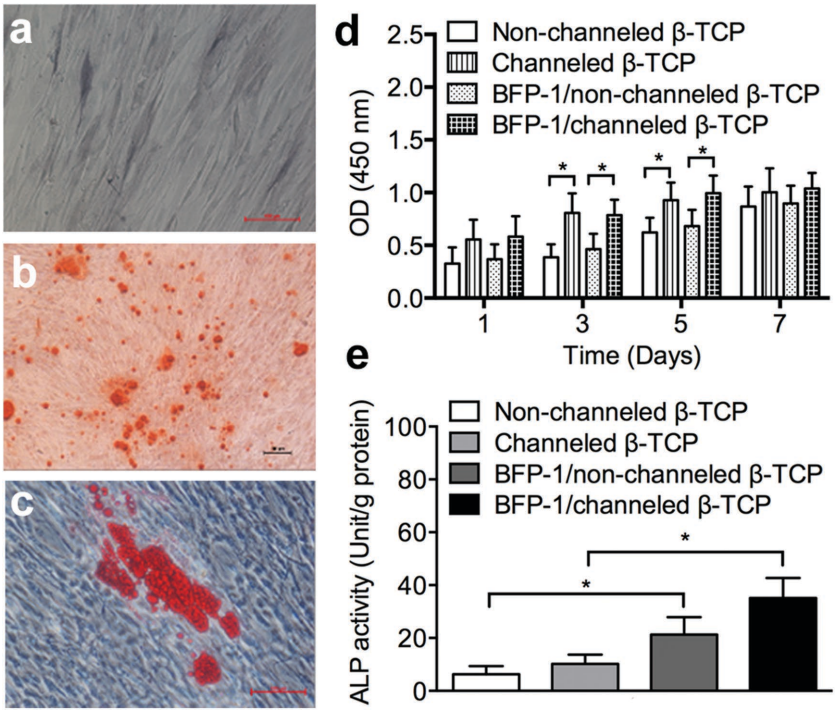


**Figure 2.** a) ALP staining, b) Alizarin red staining, and c) Oil Red O staining show that hBMSCs have osteogenic and adipogenic differentiation potential. d) Cell proliferation assay showed that channeled $\beta$-TCP scaffolds significantly promoted cell proliferation at day 3 and 5, regardless of the addition of BFP-1. e) BFP-1 increased ALP activity of hBMSCs, but there was no difference in ALP activity between the channeled and nonchanneled scaffolds.

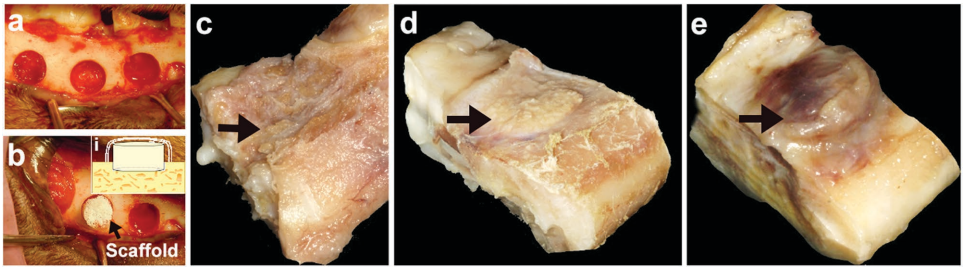


**Figure 3.** a) Bone defects with 8 mm diameter and 2 mm depth were created in the mandibular bone of beagle dogs, and b) scaffolds were implanted into the defects for 2 mm depth, and 4 mm was left outside. A tissue generation membrane was used to cover the scaffold (inset image (i)). c) Macroscopic pictures of explants show that the mandible without implant was sunken after 12 weeks (c) (The black arrow shows the position of the sunken defect). d) In the nonchanneled scaffold group, the scaffold had obvious adsorption (the black arrow shows that the original implanted scaffolds part above the defect already decreased to the same level of the host tissue). e) However, the scaffold with channels maintained the height (the black arrow shows that the upper part of the scaffold still has the height).

of scaffolds without BFP-1 (Figure 2e). There was no significant increase of ALP activity in the group without BFP-1, and there was no difference between groups of channeled and nonchanneled scaffolds. These results collectively implied that channels have a role in cell proliferation but not in the differentiation of stem cells.

### 2.4. In Vivo Implantation and Histological Characterization

To further verify the ability of channels in the porous scaffold to promote bone formation, we created mandibular bone defects (**Figure 3**a), and implanted scaffolds into the defective sites 2 mm, leaving 4 mm outside of the defects (Figure 3b), and an absorbable membrane was used to cover the implanted scaffold (insert i). After 4 or 12 weeks, we harvested the implanted tissues. Macroscopic observation of samples from 12 weeks postsurgery indicated that the bone sites in the group with no implants had sunken collapse (Figure 3c). Nonchanneled scaffolds had partial absorption, and the outside height of the bone surface was slightly decreased (Figure 3d). However, the height of channeled scaffolds in the implanted sites was maintained (Figure 3e). The H&E staining of the samples revealed all the implanted scaffolds were tightly bound and integrated to the mandible bed, and no evident inflammation was found in any of the samples postsurgery (**Figure 4**, highlighted in the yellow rectangle box). The newly regenerated tissue in channeled scaffold group augmented much more tissue volume of mandible compared with that of nonchanneled scaffold group. Masson trichrome staining of all the samples presented a wide range of blue stained collagen distributed in the newly regenerated tissue, which indicated the immaturity of new regenerated tissue (**Figure 5**). In the channeled group, more blue-to-red stained collagens in the defective zones were observed compared to the two groups, which implied that the maturity degree of mineralized collagen was higher in channeled scaffolds than that of nonchanneled scaffolds.

### 2.5. Vascularization in the Scaffolds

To observe the new formation of blood vessels in the implanted scaffolds, we used the immunohistochemistry staining of CD34 and CD 105. The results indicated that brown lumens presented in channeled scaffolds were significantly more than that in nonchanneled scaffold and no-implant groups (**Figure 6**). After quantitative assay based on CD105 immunohistochemistry staining results, the number of blood vessels formed in the channeled scaffolds was significantly higher than that in the other two groups after 4 weeks' implantation (**Figure 7**a). To observe the difference in the number of formed blood vessels between different height of the scaffold, virtual three layers were divided from the bone bed to the top of the scaffold: lower, middle, and upper layer. The numbers of blood vessels formed in the three different layers showed that there was significant difference between the channeled scaffold group ($3.6 \pm 1.3$) and nonchanneled scaffold group ($1.5 \pm 1.0$) in the middle layer ($p < 0.05$), while there was no significant difference in lower layer and upper layer. There was a decreasing trend of the number of blood vessels from the bone bed to the top of the newly regenerated tissue (Figure 7b). This result remarkably implies that the channels promoted the vertical growth of host vasculature from the bottom of the bone bed into the porous scaffolds. The growth of blood vessels provides nutrition for new bone formation, which maintained the height of the bone and the shape of the porous scaffolds.

### 2.6. Micro-CT

To observe new bone formation in the scaffolds, we used micro-CT scanning to compare new bone height in the three groups. After 4 weeks postsurgery, there were few bone tissues formed in the nonimplanted group. At 12 weeks, the height of the bone did not significantly increase. In the nonchanneled scaffold group, after 4 weeks, the edge of the scaffold started to degrade. Interestingly, there was no scaffold part left outside of the host mandibular bone at 12 weeks. Scaffolds showed remarkable absorption. However, in the channeled scaffold group, after 12 weeks, the scaffold still maintained the height, and mineralized matrices were observed (**Figure 8**a). After quantitative assay, the height of new regenerated tissue in channeled $\beta$-TCP scaffolds at 4 weeks was 5.05 mm, and that in nonchanneled scaffolds was 4.83 mm. There was no significant difference, but both of them were significantly higher than that in the blank control group (0.29 mm) ($p < 0.05$) (Figure 8b). However, after 12 weeks,




DOI: 10.1002/adfm.201602631

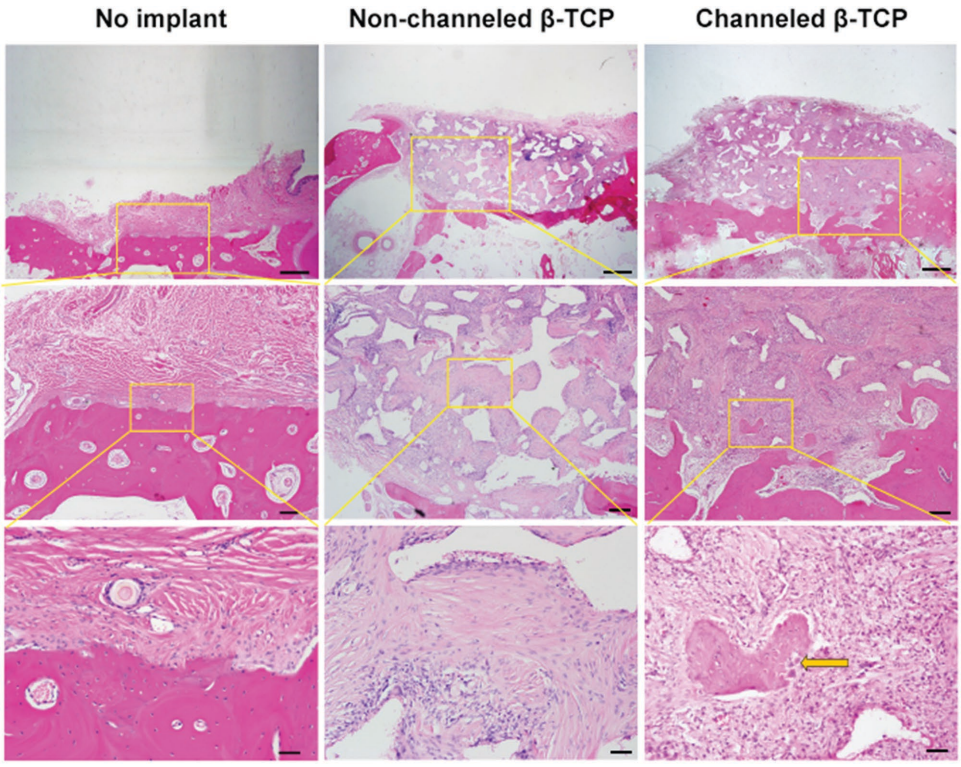


**Figure 4.** Hematoxylin and eosin (H&E) staining shows the structure of newly formed bone in the three groups. The implanted scaffolds were tightly bound and integrated to the mandible bed. (From the yellow rectangular box, it shows that there is no gap seen between the two different pink colors. The deep pink color shows the host bone bed), and no evident inflammation was found in any of the samples postsurgery. Obviously, channeled scaffolds promoted the better bone structure compared to the other groups, as more deep pink can be observed. The scale bars in the first, second, and third rows are 1 mm, 200 μm, and 50 μm, respectively. The yellow arrow shows the new bone tissue formation with blood vessels.

the height of newly formed bone tissue in the channeled scaffold group (4.75 ± 0.57 mm) was significantly higher than that in the nonchanneled scaffold group (2.61 ± 0.51 mm), and in the blank control group (0.85 ± 0.33 mm) ($p < 0.05$) (Figure 8b).

Analogously, bone volume percentage between the channeled scaffold group (8.4 ± 2.4%) and nonchanneled scaffold group (7.6 ± 2.7%) was not significantly different, but significantly higher than that of the blank control group (0.29 ± 0.28) after four weeks postsurgery ($p < 0.05$). However, the percentage of bone volume (BV)/total volume (TV) in the channeled scaffold group (14.9 ± 1.6%) was significantly higher than that in the nonchanneled group (10.3 ± 1.9%) and that in the blank control group (5.3 ± 2.1%) after twelve weeks postsurgery ($p < 0.05$) (Figure 8c). Surprisingly, there was no significant difference of bone mineral density (BMD) among the three groups, both 4 and 12 weeks postsurgery (Figure 8d).

These results in animals showed that channeled scaffolds could hold the height of new regenerated bone and promote vascular growth on bone augmentation. However, the channeled scaffolds had no significant influence on bone density compared with the nonchanneled scaffolds. The new regenerated bone was mainly consisting of immature bone. New experiments about how to enhance the quality and structure of new bone are required.

These results show that the channel structure of the macroporous scaffold played a critical role in promoting vascularization. Therefore, it is not surprising that the fabrication of scaffolds has become to precisely control its construction. Computer-aided design will play a more important role in designing the inner structure of scaffolds, especially for microvessel channels. It will come true that fabrication of scaffolds can accurately reproduce the detailed data of native bone tissue structure, including porosity, mechanical strength, vessel channels, and so on.[42,43] Future studies will imitate the complex native bone structure in detail to reproduce a fine microenvironment of bone regeneration for cell adhesion, proliferation, migration, differentiation, and function.

## 3. Conclusions

In summary, our unique technique has a promising potential to produce multiple channels within a macroporous bioceramic scaffold. Channeled scaffolds had significantly higher degradation rate compared to nonchanneled scaffolds. Channeled scaffolds did not promote ALP production of hBMSCs, but BFP-1 did. However, channeled scaffolds accelerated cell proliferation in vitro, promoted the ingrowth of host vasculature in vivo, and maintained the height of newly formed bone. The bone density of newly formed bone in nonchanneled and channeled scaffolds had no difference. The ability of channeled scaffolds to promote vascular growth and further new bone formation in dog bone defects brought promising potential for mandibular bone augmentation, even for craniofacial bone regeneration.

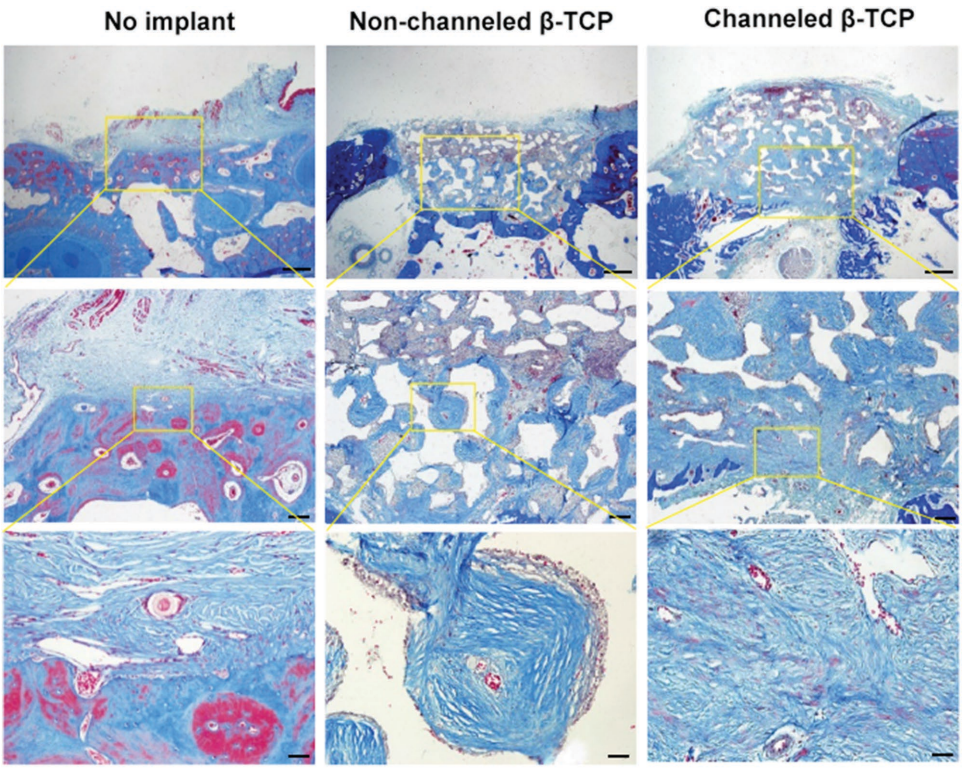


**Figure 5.** Masson trichrome staining shows the mineralized degree of bone matrix collagen. In the host bone part, deep blue and red colors are seen. In nonimplanted and nonchanneled groups, the light blue is distributed in the newly regenerated tissue, which indicated the immaturity of new regenerated tissue. In the channeled group, more blue-to-red stained collagens in the defective zones were observed compared to the two groups, which implies that more mature bone matrix formed. The scale bars in the first, second, and third rows are 1 mm, 200 μm, and 50 μm, respectively.

## 4. Experimental Section

*Preparation of Hollow-Channeled Porous β-TCP Scaffolds*: Briefly, β-TCP nano-powder purchased from Nanocerox Inc. (Ann Arbor, MI), carboxymethyl cellulose powder, dispersant (Darvan C), and surfactant (Surfonals) were mixed with distilled water while stirring to form the β-TCP slurry.[35] Paraffin beads were filled in customized channeled molds and partially melted. Afterwards, β-TCP slurry was cast into the paraffin-filled mold and then solidified and completely dried. After demolding the casted body, the β-TCP green-bodies were sintered at high temperature in a muffle furnace for three hours. Thus, porous β-TCP scaffolds with and without hollow channels were produced. The scaffolds were cylindrical, 8 mm in diameter, and 6 mm in height. The diameter size of the hollow channels was 1 mm (Figure 1). The number of five hollow channels in the scaffolds was determined by the diameter of the scaffolds. The hollow channels were distributed in the scaffolds. The total porosity and mechanical properties of the scaffolds were reported in our previous studies.[34,44,45] The pore morphology was observed by scanning electronic microscopy according to our previous study.[35]

*In Vitro Degradation of Scaffolds*: The dissolution rate of the scaffolds was tested by measuring the concentration of phosphate acid ions ($PO^{3-}_4$) in a Tris buffer according to our published paper.[46] Briefly, each scaffold was separately soaked in 1 M sterile Tris buffer (pH 7.4) at a fixed ratio of scaffold to buffer at 1 g:100 mL, and kept in sealed containers and maintained at 37 °C. At 1, 3, 5, 7, 14, 21, and 28 d, 500 μL aliquot of the solutions was taken out for analysis and equal fresh buffer was added to keep the constant volume. Phosphate ions concentration was measured using the malachite green phosphate detection kit (R&D systems).

*Loading BFP-1 onto Scaffolds*: The BFP-1 powder (synthesized by SBS Genetech Corporation, Beijing, China) was centrifuged and dissolved in phosphate buffer solution at the concentration of 200 μg $mL^{-1}$. Scaffolds including channeled and nonchanneled scaffolds were sterilized using $^{60}Co$ radiation. One hundred microliter BFP-1 solution was loaded into each sterilized scaffold, and the scaffolds were incubated in BFP-1 solution overnight at 4 °C.

To study the in vitro release profile of BFP-1 from the scaffolds, the BFP-1-loaded scaffolds were put into a vial containing 2 mL phosphate-buffered saline (PBS). The vials were incubated at 37 °C for 7 d with gentle shaking. At the end of each time point, the released medium was collected, and the same amount of fresh culture media was added to the vial in order to maintain the constant volume of the medium. The amount of released BFP-1 was measured using a BFP-1 enzyme-linked immunosorbent assay (ELISA) kit. The release profile was calculated in terms of the cumulative release percentage of BFP-1 (%, w/w) with incubation time. Four scaffolds per group at each time point were carried out.

*hBMSC Culture and Osteogenic Differentiation*: hBMSCs culture was established from the redundant cancellous bone amputated during orthognathic surgery in Peking University Hospital of Stomatology. The suspension collected from the vibration of cancellous bone in alpha-modified minimum essential media (α-MEM, Gbico, USA) was centrifuged at 1000 rpm for 5 min. After removing the supernatant, the cells were resuspended and cultured in α-MEM supplemented with 10% fetal bovine serum (Gbico, USA) and 1% penicillin (10 000 U $mL^{-1}$) and streptomycin (10 mg $mL^{-1}$) (P/S, Gbico, USA) under standard conditions (37 °C, 95% air humidity, 5% $CO_2$). Institutional Review Board of Peking University School of Stomatology approved this method (PKUSSIRB-201520020).

The hBMSCs were seeded in 6-well plates with the osteogenic differentiation media (α-MEM, 10% fetal bovine serum, 1% penicillin-streptomycin, 50 mg $mL^{-1}$ ascorbic acid, $10 \times 10^{-3}$ M glycerol-2-phosphate, and $100 \times 10^{-9}$ M dexamethasone). The ALP of the cells was determined by staining with the ALP stain kit (Jiangcheng Bioengineering Institute,




DOI: 10.1002/adfm.201602631

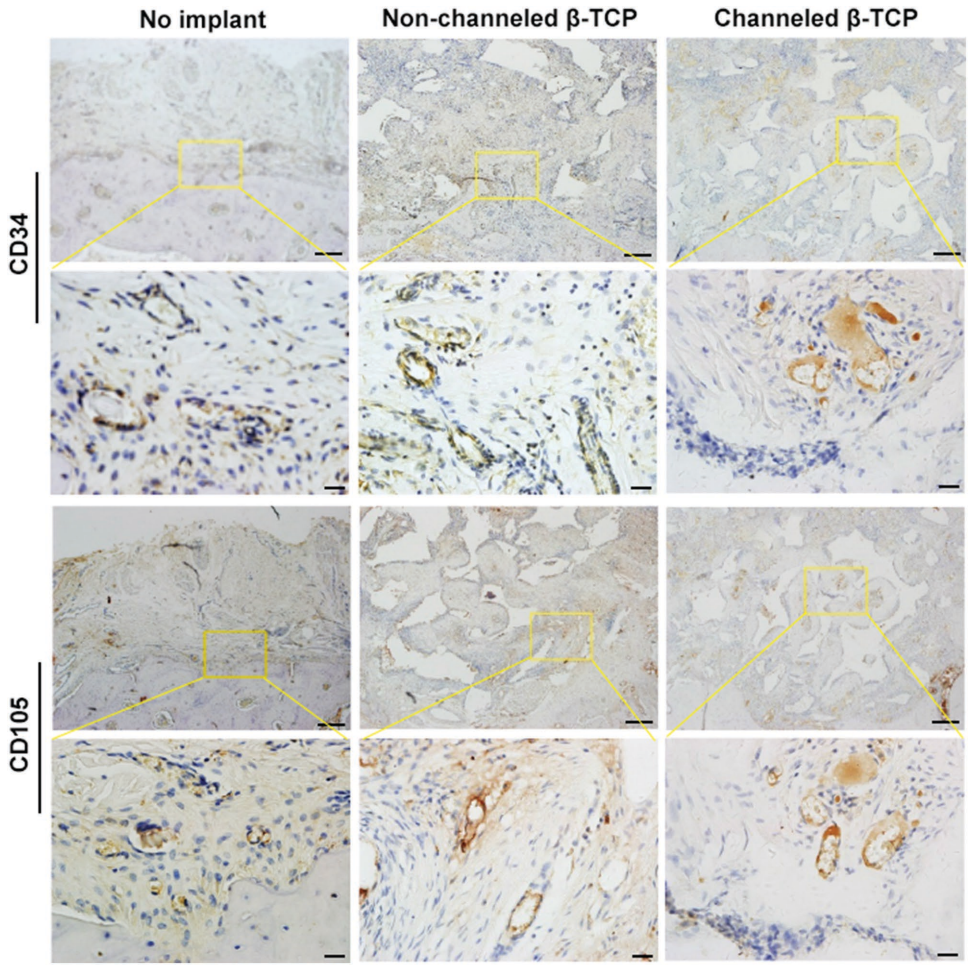


**Figure 6.** The immunohistochemistry staining of CD34 and CD105 indicates the lumen structure of newly formed blood vessels. Results show that brown lumens presented in channeled scaffolds were significantly more than that in nonchanneled scaffolds and no-implant group. The scale bars in the first and second rows of CD34 are 200 and 20 μm, respectively. The scale bars in the images of CD105 are the same.

Nanjing, China) on day 14 and the mineralized nodule was determined by staining with Alizarin red S (Sigma, USA) on day 21. On the other hand, the hBMSCs were cultured with the adipogenic differentiation media (α-MEM, 10% fetal bovine serum, 1% penicillin-streptomycin, 50 mg $mL^{-1}$ ascorbic acid, $0.5 \times 10^{-3}$ M 3-isobutyl-1-methylxanthine, $60 \times 10^{-6}$ M indomethacin, $0.5 \times 10^{-6}$ M hydrocortisone, and 10 μg $mL^{-1}$ insulin). The lipid droplet was determined by staining with Oil Red O (Sigma, USA) on day 21.

*Proliferation of hBMSCs on Scaffolds*: The proliferation of hBMSCs on scaffolds was assessed by CCK-8 assay (Dojindo, Kumamoto-ken, Japan). One hundred microliter of hBMSCs cell suspension containing $1 \times 10^4$ were loaded onto each scaffold. The cell suspension penetrated into the pores and the cells/scaffold were incubated 1 h for cell attachment, then a culture medium was added to continue to culture cells. The culture medium was changed every two days. After 1, 3, 5, and 7 d, the medium was replaced with 10% CCK-8 solution and incubated for 4 h at 37 °C. The absorbance of the formazan-dissolved solution was observed by a spectrometer at a wavelength of 450 nm.

*ALP Activity of hBMSCs on Scaffolds*: After hBMSCs were seeded onto scaffolds for 24 h, culture media was changed to an osteogenesis differentiation medium. To evaluate the ALP activity, hBMSCs were lysed with RIPA lysis buffer (Solarbio, Beijing, China). The cell lysate was then centrifuged at 12 000 g for 4 min. The ALP activity assay was performed using a para-nitrophenyl phosphate kit (Jiangcheng Bioengineering Institute, Nanjing, China).

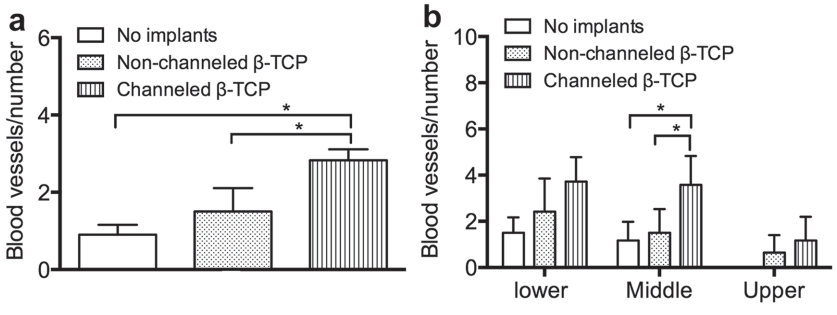


**Figure 7.** a) The number of blood vessels formed in the channeled scaffolds was significantly higher than that in the other two groups after 4 weeks' implantation. b) The numbers of blood vessels formed in three different layers from bone bed to the top of the scaffold showed significant difference.

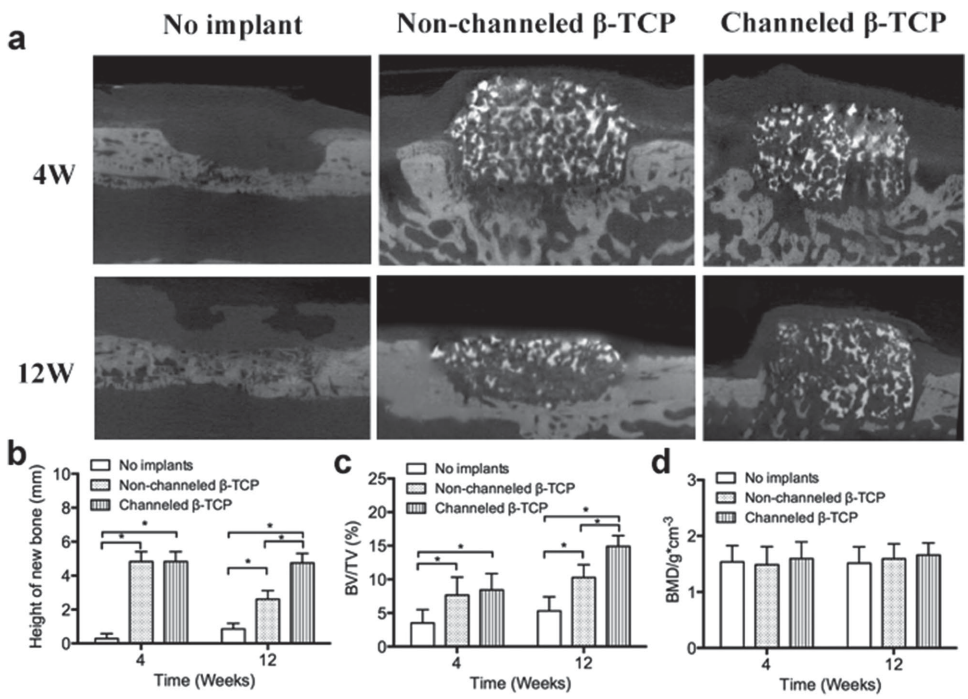


**Figure 8.** a) Micro-CT images show that channeled scaffolds can maintain the height of regenerated bone, but scaffolds without channels degraded and lowered the height. b,c) Quantitative results of the height of new bone and the ratio of BV/TV show that the channeled scaffold significantly promoted bone formation, d) though the density of new bone is not different in the three groups.

*Bone Vascularization and Augmentation In Vivo*: Three beagle dogs were used as bone augmentation models. Three experimental groups were designed as follows: (a) channeled scaffolds with BFP-1; (b) nonchanneled scaffolds with BFP-1; (c) no implant control. Each dog had four surgically defective sites on the left side of the mandible, and four on the right side. They were divided into three groups. Both sides of Dog 1 and the left side of Dog 2 were under surgery at one time, and the right side of Dog 2 and both sides of Dog 3 were under surgery 8 weeks later. Totally, each group had eight defective sites including four defective sites observed for 4 weeks and four for 12 weeks.

Each defect with 2 mm depth and 8 mm diameter in the cortical bone was created on the buccal side of the mandible of beagle dogs. Scaffolds were inserted into the defect sites. After insertion, a two-millimeter depth of the scaffolds was in the defect, and 4 mm of them was left outside. The implanted scaffolds were then covered with biological guided membranes (Lando Biomaterials Co., Ltd, Shenzhen, China) and sutured in a tension-reduced way.

All animal studies were performed in accordance with procedures approved by the Animal Care and Ethics Committee of Peking University Health Science Center (LA2014-7).

After the surgery, all dogs received antibiotics (penicillin G, 200 000 units) intramuscularly daily for 3 d. Animals were housed individually, kept in a 12 h light/dark cycle at controlled temperature (21 °C) and fed ad libitum with soft diet. Dogs were sacrificed by an overdose of sodium pentobarbital 12 weeks after the first surgery. Blood vessel formation and numbers counting from CD34 and CD105 immunohistochemistry staining were performed in the samples harvested at 4 weeks after their surgery. The samples observed for 12 weeks were harvested for osteogenesis observation.

*Histological Examination*: After fixation with 10% of phosphate-buffered formalin, the samples of mandibles were cut into two halves. The specimens were decalcified with 10% of EDTA for 12 weeks and then embedded in paraffin. The two sides of each specimen were parallel to the sectioned surface.

Those samples of 4 weeks postsurgery were used for immunohistochemistry stain of CD34 (anti-CD34 antibody, Proteintech, USA) and CD105 (anti-CD105 antibody, 10862-1-AP, Proteintech, USA) to examine the blood vessel formation in an early stage (within four weeks). In the CD105 immunohistochemistry stained section, a 6 mm high interested area based on the bone bed was divided into lower, middle, and upper layers with 2 mm height for each layer. In each layer, 6 view fields were randomly photographed in order to count vessel numbers. Serial cross-sections of decalcified specimens of bone augmentation sites at 12 weeks postsurgery were sectioned for hematoxylin and eosin (H&E) staining and Masson staining for detecting levels of new bone formation.

*Micro-CT Examination*: After the mandibular bones with implants were harvested, the mandibles were fixed with 10% formalin for three days and then underwent micro-CT scanning (Siemens Inveon, Germany) with 80 kV voltage, 500 μA current, and voxel of 9.08 μm. All data were analyzed and 3D-reconstructed by Inveon Research Workplace 4.2. An 8 mm in diameter and 6 mm in height cylinder region based on the bone bed was designated as the region of interest. The height of the newly regenerated tissue, bone volume percentage, and bone mineral density in that region were compared among the three groups.

## Acknowledgements

This work was supported by Beijing Natural Science Foundation of China (7133255), Florida Atlantic University Startup fund (CB6007), NIH R01AR057837 (NIAMS), NIH R01DE021468 (NIDCR), DOD W911NF-14-1- 0545 (DURIP), and DOD W81XWH-10-1-0966 (PRORP).

Received: May 26, 2016
Revised: July 4, 2016
Published online:

[1] S. T. Chen, T. G. Wilson Jr., C. H. Hammerle, *Int. J. Oral Maxillofac. Implants* **2004**, *19*, 12.
[2] V. Lekovic, P. M. Camargo, P. R. Klokkevold, M. Weinlaender, E. B. Kenney, B. Dimitrijevic, M. Nedic, *J. Periodontology* **1998**, *69*, 1044.
[3] J. I. Cawood, R. A. Howell, *Int. J. Oral Maxillofac. Surg.* **1991**, *20*, 75.
[4] G. Avila-Ortiz, S. Elangovan, K. W. Kramer, D. Blanchette, D. V. Dawson, *J. Dent. Res.* **2014**, *93*, 950.
[5] C. E. Nemcovsky, V. Serfaty, *J. Periodontology* **1996**, *67*, 390.
[6] H. R. Stanley, M. B. Hall, A. E. Clark, C. J. King 3rd, L. L. Hench, J. J. Berte, *Int. J. Oral Maxillofac. Implants* **1997**, *12*, 95.
[7] D. Carmagnola, P. Adriaens, T. Berglundh, *Clinical Oral Implants Res.* **2003**, *14*, 137.
[8] W. G. De Long Jr., T. A. Einhorn, K. Koval, M. McKee, W. Smith, R. Sanders, T. Watson, *J. Bone Jt. Surg., Am. Vol.* **2007**, *89*, 649.
[9] G. M. Calori, E. Mazza, M. Colombo, C. Ripamonti, *Injury* **2011**, *42 Suppl 2*, S56.
[10] A. J. Salgado, O. P. Coutinho, R. L. Reis, *Macromolecular Bioscience* **2004**, *4*, 743.
[11] C. Masaki, T. Nakamoto, T. Mukaibo, Y. Kondo, R. Hosokawa, *Journal Prosthodontic Res.* **2015**, *59*, 220.
[12] L. Wang, H. Fan, Z. Y. Zhang, A. J. Lou, G. X. Pei, S. Jiang, T. W. Mu, J. J. Qin, S. Y. Chen, D. Jin, *Biomaterials* **2010**, *31*, 9452.
[13] L. Bi, W. Cheng, H. Fan, G. Pei, *Biomaterials* **2010**, *31*, 3201.
[14] K. Rezwan, Q. Z. Chen, J. J. Blaker, A. R. Boccaccini, *Biomaterials* **2006**, *27*, 3413.
[15] J. E. Schroeder, R. Mosheiff, *Injury* **2011**, *42*, 609.
[16] F. R. Rose, R. O. Oreffo, *Biochem. Biophys. Res. Commun.* **2002**, *292*, 1.
[17] J. Yang, Y. Kang, C. Browne, T. Jiang, Y. Yang, *J. Craniofacial Surg.* **2015**, *26*, e148.
[18] E. C. Novosel, C. Kleinhans, P. J. Kluger, *Adv. Drug Delivery Rev.* **2011**, *63*, 300.
[19] M. W. Laschke, M. D. Menger, *Eur. Surg. Res.* **2012**, *48*, 85.
[20] T. Takebe, N. Koike, K. Sekine, M. Enomura, Y. Chiba, Y. Ueno, Y. W. Zheng, H. Taniguchi, *Transplant. Proc.* **2012**, *44*, 1130.
[21] X. Zhao, L. Liu, J. Wang, Y. Xu, W. Zhang, G. Khang, X. Wang, *J. Tissue Eng. Regener. Med.* **2014**, DOI: 10.1002/term.1863.
[22] A. Nishiguchi, M. Matsusaki, Y. Asano, H. Shimoda, M. Akashi, *Biomaterials* **2014**, *35*, 4739.
[23] J. D. Baranski, R. R. Chaturvedi, K. R. Stevens, J. Eyckmans, B. Carvalho, R. D. Solorzano, M. T. Yang, J. S. Miller, S. N. Bhatia, C. S. Chen, *Proc. Natl. Acad. Sci. USA* **2013**, *110*, 7586.
[24] M. Shin, K. Matsuda, O. Ishii, H. Terai, M. Kaazempur-Mofrad, J. Borenstein, M. Detmar, J. P. Vacanti, *Biomed. Microdevices* **2004**, *6*, 269.
[25] R. Chang, J. Nam, W. Sun, *Tissue Eng. Part A* **2008**, *14*, 41.
[26] P. Carmeliet, R. K. Jain, *Nature* **2000**, *407*, 249.
[27] R. Y. Kannan, H. J. Salacinski, K. Sales, P. Butler, A. M. Seifalian, *Biomaterials* **2005**, *26*, 1857.
[28] R. K. Jain, P. Au, J. Tam, D. G. Duda, D. Fukumura, *Nat. Biotechnol.* **2005**, *23*, 821.
[29] J. Rnjak-Kovacina, L. S. Wray, J. M. Golinski, D. L. Kaplan, *Adv. Funct. Mater.* **2014**, *24*, 2188.
[30] L. S. Wray, J. Rnjak-Kovacina, B. B. Mandal, D. F. Schmidt, E. S. Gil, D. L. Kaplan, *Biomaterials* **2012**, *33*, 9214.
[31] Y. J. Lee, J. H. Lee, H. J. Cho, H. K. Kim, T. R. Yoon, H. Shin, *Biomaterials* **2013**, *34*, 5059.
[32] H. K. Kim, J. H. Kim, D. S. Park, K. S. Park, S. S. Kang, J. S. Lee, M. H. Jeong, T. R. Yoon, *Biomaterials* **2012**, *33*, 7057.
[33] Y. Kang, S. Kim, J. Bishop, A. Khademhosseini, Y. Yang, *Biomaterials* **2012**, *33*, 6998.
[34] Y. Kang, S. Kim, A. Khademhosseini, Y. Yang, *Biomaterials* **2011**, *32*, 6119.
[35] Y. Kang, A. Scully, D. A. Young, S. Kim, H. Tsao, M. Sen, Y. Yang, *Eur. Polymer J.* **2011**, *47*, 1569.
[36] H. Bai, D. Wang, B. Delattre, W. Gao, J. De Coninck, S. Li, A.P. Tomsia, *Acta Biomater.* **2015**, *20*, 113.
[37] M. Radisic, J. Malda, E. Epping, W. Geng, R. Langer, G. Vunjak-Novakovic, *Biotechnol. Bioeng.* **2006**, *93*, 332.
[38] M. Radisic, H. Park, F. Chen, J. E. Salazar-Lazzaro, Y. Wang, R. Dennis, R. Langer, L. E. Freed, G. Vunjak-Novakovic, *Tissue Eng.* **2006**, *12*, 2077.
[39] F. R. Rose, L. A. Cyster, D. M. Grant, C. A. Scotchford, S. M. Howdle, K. M. Shakesheff, *Biomaterials* **2004**, *25*, 5507.
[40] B. Sharaf, C. B. Faris, H. Abukawa, S. M. Susarla, J. P. Vacanti, L. B. Kaban, M. J. Troulis, *J. Oral. Maxillofac. Surg.* **2012**, *70*, 647.
[41] W. A. Castelli, D. F. Huelke, *Am. J. Anat.* **1965**, *116*, 149.
[42] J. A. Inzana, D. Olvera, S. M. Fuller, J. P. Kelly, O. A. Graeve, E. M. Schwarz, S. L. Kates, H. A. Awad, *Biomaterials* **2014**, *35*, 4026.
[43] J. Wang, M. Yang, Y. Zhu, L. Wang, A. P. Tomsia, C. Mao, *Adv. Mater.* **2014**, *26*, 4961.
[44] Y. Kang, N. Mochizuki, A. Khademhosseini, J. Fukuda, Y. Yang, *Acta Biomater.* **2015**, *11*, 449.
[45] Y. Kang, L. Ren, Y. Yang, *ACS Appl. Mater. Interfaces* **2014**, *6*, 9622.
[46] Y. Kang, S. Kim, M. Fahrenholtz, A. Khademhosseini, Y. Yang, *Acta Biomater.* **2013**, *9*, 4906.